Acta Crystallographica Section D
Biological Crystallography
ISSN 0907-4449

Cross-protomer interaction with the photoactive site in oligomeric proteorhodopsin complexes

Tingting Ran,[a]‡ Gabriel Ozorowski,[b,c]‡ Yanyan Gao,[a]‡ Oleg A. Sineshchekov,[d] Weiwu Wang,[a]* John L. Spudich[d]* and Hartmut Luecke[b,c,e,f,g]*

[a]Key Laboratory of Agricultural and Environmental Microbiology, Ministry of Agriculture, College of Life Sciences, Nanjing Agricultural University, Nanjing 210095, People's Republic of China, [b]Department of Molecular Biology and Biochemistry, University of California, Irvine, Irvine, CA 92697, USA, [c]Center for Biomembrane Systems, University of California, Irvine, Irvine, CA 92697, USA, [d]Center for Membrane Biology, Department of Biochemistry and Molecular Biology, University of Texas Medical School, Houston, TX 77030, USA, [e]Department of Physiology and Biophysics, University of California, Irvine, Irvine, CA 92697, USA, [f]Department of Computer Science, University of California, Irvine, Irvine, CA 92697, USA, and [g]Unidad de Biofisica (CSIC, UPV/EHU) and Departamento de Bioquimica, Universidad del Pais Vasco, 48940 Leioa, Spain

‡ These authors contributed equally to this work.

Correspondence e-mail: wwwang@njau.edu.cn, john.l.spudich@uth.tmc.edu, hudel@uci.edu

Received 11 May 2013
Accepted 26 June 2013

PDB References:
*Med12*BPR, 4jq6;
*HOT75*BPR D97N, 4kly;
*HOT75*BPR D97N/Q105L, 4knf

Proteorhodopsins (PRs), members of the microbial rhodopsin superfamily of seven-transmembrane-helix proteins that use retinal chromophores, comprise the largest subfamily of rhodopsins, yet very little structural information is available. PRs are ubiquitous throughout the biosphere and their genes have been sequenced in numerous species of bacteria. They have been shown to exhibit ion-pumping activity like their archaeal homolog bacteriorhodopsin (BR). Here, the first crystal structure of a proteorhodopsin, that of a blue-light-absorbing proteorhodopsin (BPR) isolated from the Mediterranean Sea at a depth of 12 m (*Med12*BPR), is reported. Six molecules of *Med12*BPR form a doughnut-shaped C_6 hexameric ring, unlike BR, which forms a trimer. Furthermore, the structures of two mutants of a related BPR isolated from the Pacific Ocean near Hawaii at a depth of 75 m (*HOT75*BPR), which show a C_5 pentameric arrangement, are reported. In all three structures the retinal polyene chain is shifted towards helix *C* when compared with other microbial rhodopsins, and the putative proton-release group in BPR differs significantly from those of BR and xanthorhodopsin (XR). The most striking feature of proteorhodopsin is the position of the conserved active-site histidine (His75, also found in XR), which forms a hydrogen bond to the proton acceptor from the same molecule (Asp97) and also to Trp34 of a neighboring protomer. Trp34 may function by stabilizing His75 in a conformation that favors a deprotonated Asp97 in the dark state, and suggests cooperative behavior between protomers when the protein is in an oligomeric form. Mutation-induced alterations in proton transfers in the BPR photocycle in *Escherichia coli* cells provide evidence for a similar cross-protomer interaction of BPR in living cells and a functional role of the inter-protomer Trp34–His75 interaction in ion transport. Finally, Wat402, a key molecule responsible for proton translocation between the Schiff base and the proton acceptor in BR, appears to be absent in PR, suggesting that the ion-transfer mechanism may differ between PR and BR.

1. Introduction

Proteorhodopsins (PRs), members of the microbial rhodopsin superfamily of seven-transmembrane-helix proteins that use retinal chromophores, comprise the largest subfamily of rhodopsins (Spudich *et al.*, 2000). PRs form a distinct group sharing less than 30% sequence identity with archaeal rhodopsins such as bacteriorhodopsin (BR), sensory rhodopsins I and II and halorhodopsin (Béjà *et al.*, 2000). Since the first proteorhodopsin was reported 12 years ago, more than 3200 proteorhodopsin gene sequences have been deposited in the GenBank database. PR-bearing bacteria have been shown

to account for 13% of the total bacteria in sea surface water, with an average of 25 000 PR molecules per cell (Sabehi *et al.*, 2005). Proteorhodopsins are classed into two major groups according to the wavelength of the maximum light absorption at physiological pH (Béjà *et al.*, 2001): blue-light-absorbing proteorhodopsins (BPRs) and green-light-absorbing proteorhodopsins (GPRs). A single residue change, a leucine (GPR) to a glutamine (BPR) at position 105, has been shown to be responsible for the differences in spectral tuning between the two groups (Man *et al.*, 2003). Despite this difference, numerous key residues remain conserved between the two subfamilies.

During the light-driven ion-translocation process, two crucial residues, Asp97 and Glu108, have been demonstrated to act as the primary Schiff-base proton acceptor and donor, respectively, in PRs (Dioumaev *et al.*, 2002; Wang *et al.*, 2003). In contreast to the low pK_a of the counterion in bacteriorhodopsin, the pK_a of the counterion in proteorhodopsins is generally much higher (near pH 7). Previous results showed that the conserved His75 affects the pK_a of the counterion Asp97 in proteorhodopsins (Balashov *et al.*, 2012; Hempelmann *et al.*, 2011; Bergo *et al.*, 2009) and xanthorhodopsin (His62; Luecke *et al.*, 2008).

To reveal the mechanism of light harvesting and ion translocation, it is necessary to determine the high-resolution three-dimensional structure of PR. Various approaches have been taken to gain an understanding of PR structures, including electron microscopy and solid-state NMR of two-dimensional crystals (Shastri *et al.*, 2007), which revealed hexagonal protein packing of GPR with a proposed trimeric assembly. Single-molecule microscopy and spectroscopy of two-dimensional crystals and the noncrystalline areas of reconstituted membrane patches also revealed GPR assembling dominantly into hexameric oligomers, with a small fraction assembling into pentamers (Klyszejko *et al.*, 2008). Some insight has been gained regarding the structural organization of the PR oligomers by site-directed spin-labeling together with electron spin-resonance line-shape and Overhauser dynamic nuclear polarization analysis (Stone *et al.*, 2013).

Three-dimensional solid-state NMR studies by Shi and coworkers assigned 153 of 248 residues by NMR ^{13}C and ^{15}N isotopic labels, established the protonation states of several carboxylic acids and detected secondary-structure elements in loops (Shi, Ahmed *et al.*, 2009; Shi, Lake *et al.*, 2009). Most recently, the *de novo* structure of GPR was reported by solution NMR spectroscopy (Reckel *et al.*, 2011), revealing a *B*–*C* loop different from other microbial rhodopsins. To date, no crystal structure of a proteorhodopsin molecule has been published. Here, we report the 2.31 Å resolution crystal structure of native BPR from an uncultured sample previously isolated from the Mediterranean Sea at a depth of 12 m (*Med12*BPR; GenBank AAY68058.1) together with the structures of two engineered mutants of a related BPR isolated from the Pacific Ocean near Hawaii at a depth of 75 m (*HOT75*BPR; GenBank AAK30179.1). These high-resolution structures coupled with functional assays provide novel insights regarding oligomeric assembly, inter-protomer communication and ion translocation in proteorhodopsins when compared with BR.

2. Materials and methods

2.1. Protein production, crystallization, data collection and processing

Details of the production and crystallization of *HOT75*BPR D97N and D97N/Q105L have been published previously (Wang *et al.*, 2012). The gene encoding the *Med12*BPR apoprotein was cloned into the pET28a vector to create the expression construct. *Med*12BPR was produced in *Escherichia coli* C43(DE3) cells with the recombinant plasmid in LB medium with 30 mg ml^{-1} kanamycin to an OD$_{600}$ of 1.0 at 310 K. The culture was induced by adding 0.5 m*M* isopropyl β-D-1-thiogalactopyranoside (IPTG) together with 5 μ*M* all-*trans* retinal. The cells were harvested by centrifugation (5000 rev min^{-1} for 10 min; Sorvall rotor F10S 6X500Y) after induction at 303 K for 3 h. The protein was purified as described by Bergo *et al.* (2009), except that the detergent was *n*-decyl-β-D-maltoside (β-DM; Anatrace). The protein was desalted and concentrated to 10 mg ml^{-1} for crystallization trials in bicelles.

Crystals of the *HOT75*BPR mutants were obtained as reported previously (Wang *et al.*, 2012). In summary, 360 frames were collected for each *HOT75*BPR mutant (1° image width) at Shanghai Synchrotron Radiation Facility and SeMet *HOT75*BPR D97N crystals were used to perform *ab initio* experimental single-wavelength anomalous dispersion (SAD) phasing. Anomalous diffraction data sets were indexed and integrated using *XDS* (Kabsch, 2010). F_A values were calculated using *SHELXC* (Sheldrick, 2008). 51 heavy-atom sites were found using *SHELXD* (Schneider & Sheldrick, 2002). The correct hand for the substructure was determined using *SHELXE* (Sheldrick, 2010). An initial model was built manually into the experimental electron-density map using *Coot* (Emsley *et al.*, 2010). This model was then used for molecular replacement for both *HOT75*BPR D97N/Q105L and *Med12*BPR.

*Med12*BPR crystals were grown using the bicelle method (Faham & Bowie, 2002) in crystallization buffer with 32%(*v*/*v*) (±)-2-methyl-2,4-pentanediol, 100 m*M* sodium acetate pH 4.5, 20 m*M* calcium chloride. Hexagonal plate crystals appeared after one week and grew to full size in 1–2 months. The crystals were immersed into Paratone-N (Hampton Research, Aliso Viejo, California, USA) and were then directly picked up in nylon loops and flash-cooled in liquid nitrogen. Crystals of Med*12*BPR diffracted to 2.30 Å resolution and 360 frames were collected (1° width) on beamline X06 of the Swiss Light Source at 100 K. The images were processed using *XDS*. Molecular replacement using the previously solved *HOT75*BPR D97N structure as a model was performed with *Phaser* (McCoy *et al.*, 2007), which successfully placed three copies of the search model. Model adjustment was performed using the program *Coot* (Emsley *et al.*, 2010) and further refinement was performed using *PHENIX* (Adams *et al.*,

Table 1
X-ray diffraction data-reduction and refinement statistics.

Values in parentheses are for the highest resolution shell.

	*Med12*BPR	*HOT75*BPR D97N	*HOT75*BPR D97N/Q105L
Data collection			
Radiation source	Beamline X06, SLS	Beamline BL17U1, SSRF	Beamline BL17U1, SSRF
Wavelength (Å)	0.979	0.979	0.979
Space group	*I*2	$P2_12_12$	$P2_12_12$
Unit-cell parameters			
a (Å)	87.2	162.1	161.4
b (Å)	101.9	168.8	168.9
c (Å)	87.3	65.7	65.7
β (°)	119.5	90.0	90.0
No. of molecules in the asymmetric unit	3	5	5
Resolution range (Å)	38.01–2.30	20.00–2.72	20.00–2.72
Total observations	142509	532319	341531
Unique reflections	28614	48838	48405
Multiplicity	5.0 (4.0)	10.9 (11.2)	7.1 (7.1)
Completeness (%)	98.3 (90.1)	99.6 (99.9)	98.5 (98.6)
R_{merge} (%)	9.2 (71.7)	22.7 (311.6)	10.5 (112.0)
Average $I/\sigma(I)$	11.3 (1.9)	8.1 (1.0)	11.3 (1.8)
Data-processing program	*XDS*	*XDS*	*XDS*
Refinement			
Refinement programs	*PHENIX*, *REFMAC*5	*PHENIX*, *REFMAC*5	*PHENIX*, *REFMAC*5
Resolution range (Å)	21.16–2.30	20.0–2.70	20.0–2.60
R factor (%)	20.8	20.9	22.2
R_{free}† (%)	26.6	26.1	26.6
R.m.s.d. stereochemistry‡			
Bond lengths (Å)	0.008	0.011	0.009
Bond angles (°)	1.48	1.66	1.59
Solvent content (%)	43.6	63.4	62.9
No. of atoms			
Protein	4812	8724	8747
Waters	13	13	11
Retinal	60	100	100
Average *B* (Å^2)			
Protein	23.2	71.4	72.7
Waters	39.0	75.0	70.3
Retinal	37.1	70.8	68.6
Ramachandran plot§ (%)			
Preferred	95.6	93.5	93.6
Allowed	4.4	6.5	6.2
Generously allowed	0.0	0.0	0.2
Outliers	0.0	0.0	0.0
PDB code	4jq6	4kly	4knf

† R_{free} based on a test-set size of 5% of all structure factors. ‡ R.m.s.d. stereochemistry is the deviation from ideal values. § Ramachandran analysis was carried out using *PROCHECK* (Laskowski *et al.*, 1993).

2010) and *REFMAC*5 (Winn *et al.*, 2011). The crystallographic statistics are summarized in Table 1.

3. Results

3.1. Crystallization

Crystals of wild-type *Med12*BPR were obtained using the bicelle method (Faham & Bowie, 2002); they belonged to space group *I*2 (*C*2 variant) and formed type I membrane-protein crystals (Michel, 1983), which are composed of stacks of two-dimensional crystalline bilayers (Fig. 1*a*). In these crystals all protomers are inserted into each stacked bilayer in a parallel fashion. Each layer has an average height of 51 Å, and the closest distance between layers is 5.5 Å.

In contrast, crystals of the D97N single-mutant and D97N/Q105L double-mutant crystals of *HOT75*BPR were obtained using standard vapor diffusion of detergent-solubilized *HOT75*BPR. Surprisingly, these crystals also formed a type I arrangement (Michel, 1983) and belonged to space group $P2_12_12$ (Fig. 1*b*). In contrast to the *Med12*BPR crystals, two pentamers form a decamer, which packs against the adjacent decamers with a nonphysiological antiparallel orientation in a single bilayer, with an increased bilayer height of 65 Å. In addition, the layers are not stacked as tightly as in *Med12*BPR, with a minimal interlayer separation of ~9 Å.

3.2. Overall crystal structure of blue proteorhodopsin and oligomer arrangement

Similar to other rhodopsin structures, the overall structure of the PR protomer is mainly comprised of seven transmembrane (TM) helices with the retinal bound covalently to Lys231 [Lys213 in *Med12*BPR; from here on, residues will be numbered according to GPR (Swiss-Prot Q9F7P4.1) and a number in parentheses will refer to numbering in *Med12*BPR, a shorter proteorhodopsin variant]. *Med12*BPR assembles into C_6 hexamers, in which the asymmetric unit contains three molecules or half a hexamer, with the crystallographic twofold axis oriented perpendicular to the bilayer generating the hexamer, in a manner very similar to the recently reported C_6 hexamer of the pH-gated *Helicobacter pylori* urea channel (Strugatsky *et al.*, 2013). In contrast, both mutants of *HOT75*BPR assemble into C_5 pentamers.

The hexameric arrangement of *Med12*BPR results in a central pore of roughly uniform diameter (20 Å) from the cytosolic to the periplasmic side (Fig. 2, left). The *HOT75*BPR pentamer forms a funnel-shaped structure also with a pore at the center, but the pore is asymmetric with twice the diameter on the periplasmic face (28 Å) compared with that on the cytosolic side (14 Å) (Fig. 2, right). In addition to the hydrophobic interactions between the membrane-embedded portions of protomers in both BPR variants (Fig. 3, middle), the BPR crystal structures reveal additional interactions contributed by specific hydrogen bonds between adjacent protomers.

A novel intermolecular interaction is found near the periplasmic region of the protein and involves hydrogen bonding between His75(57) of one protomer and the indole NH of Trp34(16) of the neighboring chain (Fig. 4). The histidine is conserved in the proteorhodopsin family and is located very close to the counterion (~3 Å), but it is not a generally conserved feature among microbial rhodopsins, although it was observed in a short hydrogen bond to the Asp counterion in the crystal structure of xanthorhodopsin (Luecke *et al.*, 2008). Previous FTIR studies have implicated His75(57) in the proton-translocation mechanism of GPR (Bergo *et al.*, 2009). In the three pairs of unique protomer interfaces in the crystal structure (chains *A*/*B*, *B*/*C* and *C*/*A* of the hexamer), a hydrogen bond from Trp34(16) to His75(57) is present across

two interfaces (Figs. 4*a* and 4*b*) but is absent from the third interface (Fig. 4*c*). Because the indole of Trp34(16) can only act as a hydrogen-bond donor, we presume that the NE2 atom of the His75(57) imidazole ring is deprotonated in the two cases in which the His receives a hydrogen bond. In all cases, the ND1 atom of the His75(57) imidazole is likely to be protonated, acting as a hydrogen-bond donor to Asp97(79) and possibly also to the main-chain carbonyl of Val53 (Ile71 in GPR).

A hydrogen bond between His75(57) and Trp34(16) is present between all neighboring protomers (chains *A*/*B*, *B*/*C*, *C*/*D*, *D*/*E* and *E*/*A*) of the *HOT75*BPR D97N single mutant and D97N/Q105L double mutant (pentamers). Mutation of Asp97(79) to asparagine, as is the case for the *HOT75*BPR structures, appears to eliminate the hydrogen-bonding interaction with His75(57), as the distances between potential donor–acceptor pairs are greater than the typical hydrogen-bond cutoff (Fig. 4*d*). Furthermore, it is presumed that the ND1 atom of His75(57) remains protonated and the NE2 atom remains deprotonated in *HOT75*BPR, resulting in this residue accepting a hydrogen bond from Trp34(16) and donating to the main-chain carbonyl O atom of Ile71 (Val53 in *Med12*BPR).

NMR studies involving the His75–Asp97 cluster in GPR (Hempelmann *et al.*, 2011) show that His with a protonated NE2 atom (His^{NE2}) is the dominant species, resulting in a hydrogen bond between the deprotonated ND1 of His75 and a protonated carboxyl on Asp97. This model agrees with protomer *A*, in which any His75(57)–Trp34(16) hydrogen bonding is abolished (Fig. 4*c*). However, in protomer *B* of *Med12*BPR a strong (<3.0 Å) bond between ND1 of His75(57) and the main-chain carbonyl of Val53 (Ile71 in GPR) is formed, which would only be possible if His75(57) is in the neutral His^{ND1} state. The fully protonated His^{+} is not likely to be owing to the hydrogen bond between the NE2 atom of His75(57) and the indole NE1 atom of Trp34(16). The His^{NE2} tautomer is four times more favorable than the His^{ND1} tautomer, unless structural interactions stabilize the latter (Hempelmann *et al.*, 2011). The role of Trp34(16) in the hexamer of *Med12*BPR may be to help in keeping Asp97(79) in a deprotonated state until it is protonated either directly by the Schiff base or by some intermediate donor during the

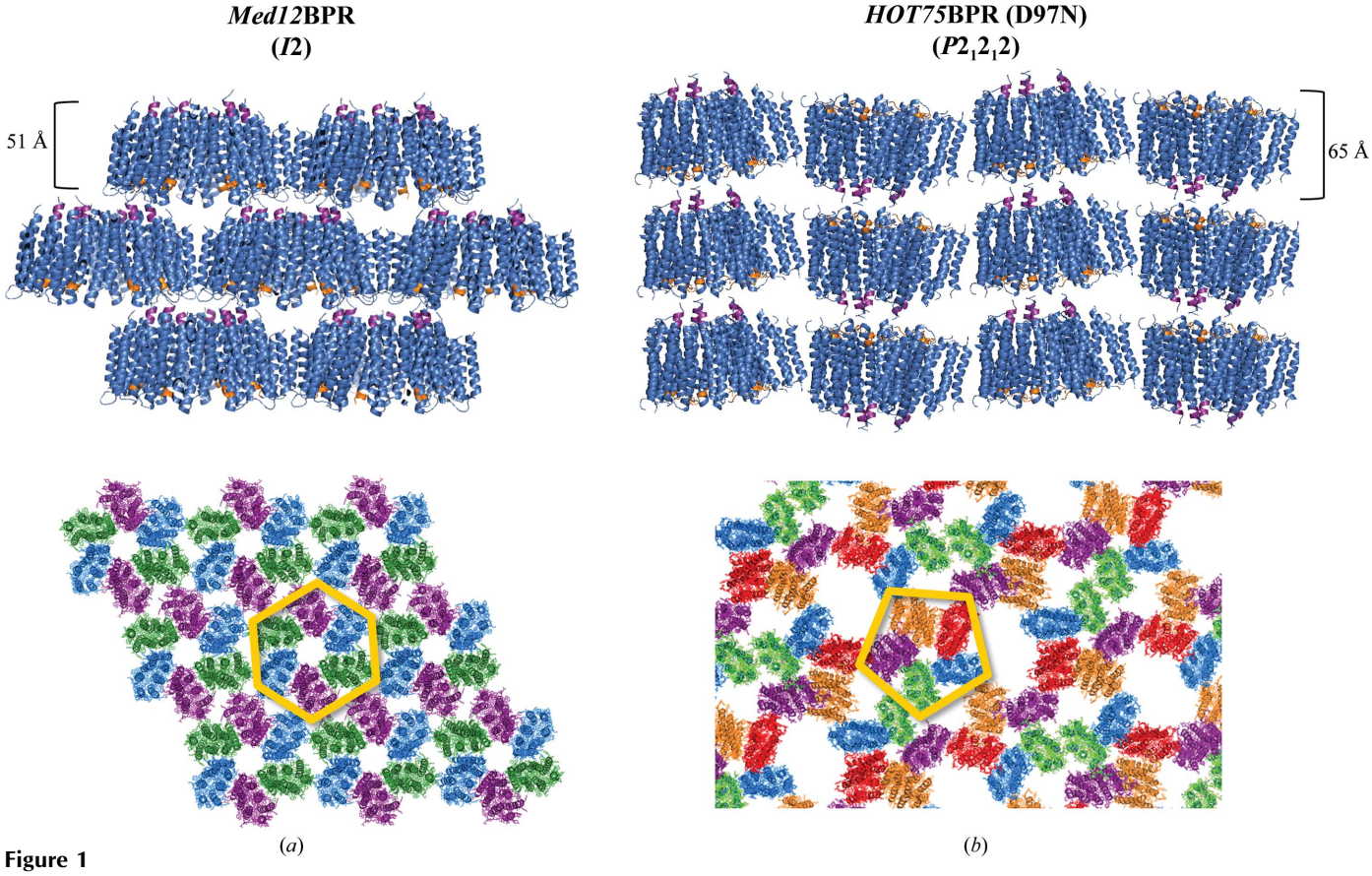

Figure 1
Crystal packing of blue-light-absorbing proteorhodopsin variants. Native *Med12* blue-light-absorbing proteorhodopsin (*Med12*BPR) crystals belonged to space group *I*2 (*C*2 variant) and are composed of type I stacks of repeating membranes containing a single layer of protein (*a*). All protomers in one layer face in the same direction. Each layer has an average height of 51 Å and the closest approach between layers is 5.5 Å. The *HOT75* D97N variant of blue-light-absorbing proteorhodopsin (*HOT75*BPR D97N) also forms type I membrane-protein crystals, which belonged to space group $P2_12_12$ (*b*). In contrast to native BPR, these layers exhibit an alternating (nonphysiological) protomer direction and have a larger height of 65 Å. In addition, the layers are not as tightly stacked, with the closest interlayer contacts having a distance of about 9 Å. The first five residues of the N-terminus of each protein have been colored orange; the final five residues of the C-terminus of each protein have been colored magenta. The figures were generated with *PyMOL* (v.1.3r1; Schrödinger).

photocycle. Assuming that His75(57) adopts one of the two possible neutral states, hydrogen bonding between Trp34(16) and the NE2 atom of His75(57) will ensure that ND1 is protonated and favors the His^{ND1} tautomer. This in turn will favor hydrogen bonding to Asp97(79) only if it is deprotonated. Without a hydrogen-bond donor for the NE2 of His75(57), the energetically most favorable species within the pH range 6–9 would call for a protonated histidine NE2 and a protonated aspartic acid carboxyl. Such a result would conflict with reports indicating Asp97(79) as the proton acceptor (Sineshchekov & Spudich, 2004), as it should be deprotonated in the ground state, and it has been reported that proton transport in proteorhodopsin requires that the Schiff-base counterion be anionic (Dioumaev *et al.*, 2003). The high pK_a of Asp97(79) (7.68) would also make unwanted protonation of Asp97(79) a challenge even in alkaline ocean water ($7.6 \leq pH \leq 8.2$; Emerson & Hedges, 2008).

Since the protein was crystallized at relative low pH, there are two plausible explanations for the range of conformations observed in the *Med12*BPR structure. (i) Asp97(79) was forced into a protonated form by the low pH, something that has been documented previously (Bergo *et al.*, 2009; Friedrich *et al.*, 2002). As a result, deprotonation of ND1 of His75(57) and protonation of NE2 are favored energetically, resulting in a disruption of the His–Trp interaction. (ii) The low pH value is below or near the pK_a of histidine, resulting in a fully protonated and charged state. Asp97(79) remains deprotonated and interacts with the protonated ND1 of His75(57), but the NE2 is also protonated at this pH and disrupts interaction with Trp34(16). Therefore, a type of equilibrium is seen in which some of the His75(57) residues are fully protonated (Fig. 4*c*) while other His75(57) residues are likely to be deprotonated [resulting in Trp34(16)–His75(57) distances that are still at the upper limit of hydrogen bonds: 2.98 and 3.15 Å].

In addition to the His–Trp interaction, an extensive inter-protomer hydrogen-bond network is found at the cytoplasmic interface (Fig. 3*d*). Arg51(33) of one protomer forms a salt bridge to the carboxylate side chains of Asp52(35) and Glu50(32) of the neighboring protomer, as well as an inter-chain hydrogen bond between the NE atom of Arg51(33) and the side-chain hydroxyl of the nearby Thr63(45). The network is further strengthened by hydrogen bonding between Glu50(32) and both Thr63(45) and Thr60(42) of the neighboring protomer.

Unique to *HOT75*BPR, the periplasmic region features an interaction between neighboring protomers through an interface comprised of an eight-residue extension of the N-terminus plus helix *A* of one protomer and helices *B* and *C* of the adjacent protomer (Fig. 3*b*). The carboxylate group of Asp22 (absent in the *Med12*BPR) structure, found in the N-terminal region of one protomer, forms hydrogen bonds to the amide N atoms of residues Thr91(73), Val92(74) and Phe93(75) (located on helix *C*) of the neighboring protomer. *Med12*BPR lacks the N-terminal extension.

3.3. Evidence for a similar cross-protomer interaction of BPR in native living cells and a functional role of the Trp34(16)–His75(57) interaction

The oligomeric forms of crystallized BPR raise the question of whether the functional pigment in *E. coli* cells also forms

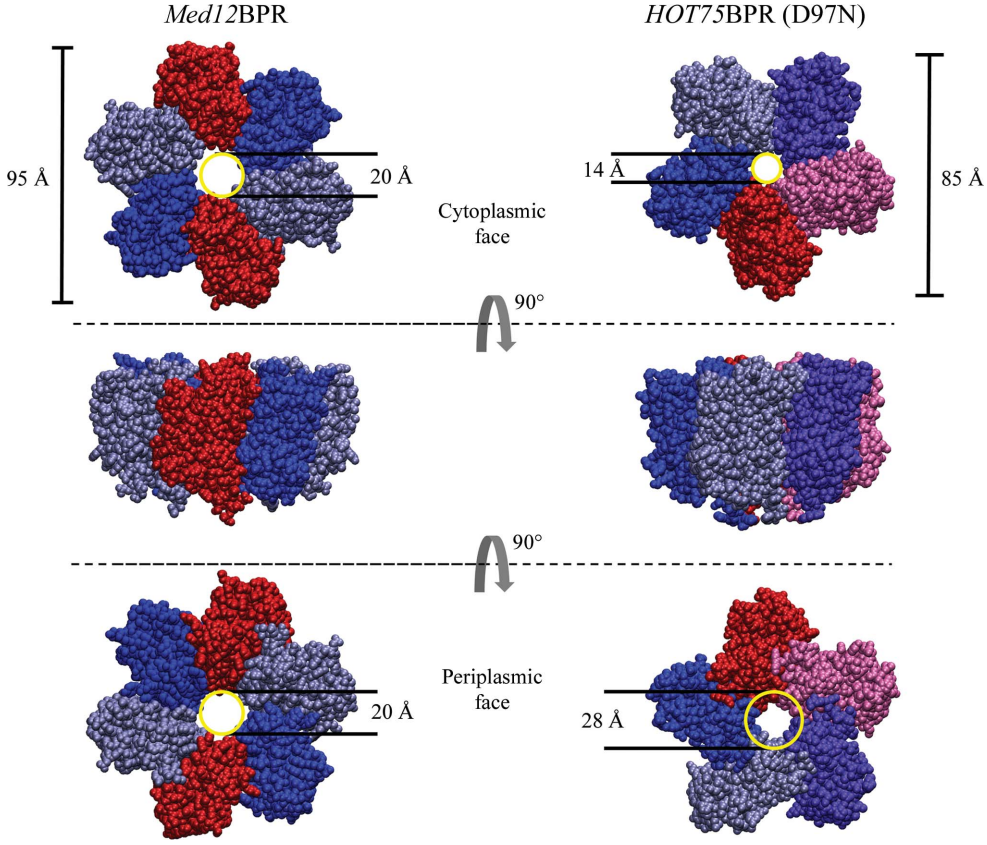

Figure 2
Multimeric assemblies of blue-light-absorbing proteorhodopsin variants. *Med12*BPR assembles as a C_6 hexameric unit, with all monomers roughly parallel to each other (middle left). A view from the cytosolic face of the hexamer (top left) reveals an inner cavity roughly 20 Å in diameter which remains uniform throughout the hexamer (bottom left). The entire assembly has a width of about 95 Å. In contrast, *HOT75*BPR exists as a C_5 pentamer with all protomers arranged in the same direction but at an angle of about 10° from the symmetry axis (middle right). A central cavity is also formed, but the diameter of 14 Å is significantly smaller than the cavity in native BPR when viewed from the cytosolic side face (top right) and enlarges to a diameter of 28 Å on the periplasmic face (bottom left). The overall width of the pentamer is about 85 Å. The figures were generated with *VMD* (Humphrey *et al.*, 1996).

oligomeric complexes. We tested whether the effects of mutations on light-induced charge movements in BPR expressed in *E. coli* cells support the presence of interacting oligomers *in vivo*. The crystal structures show that Trp34(16) in a given protomer is distant (~20 Å) from the photoactive site of the same protomer (Fig. 5), but nevertheless we observe that the mutation W34(16)D causes dramatic alterations in the photochemical function of BPR *in vivo*. The rationale of the test is that if the effect of the W34(16)D mutation depends on the interaction of His75(57) with the residue at position 34(16) (*i.e.* the introduced Asp), then mutations of His75(57) should disrupt or at least alter the interaction, causing restoration of the wild-type phenotype to some extent, *i.e.* causing suppression of the W34(16)D phenotype. Such a suppressor effect of H75(57)A on W34(16)D is observed (Fig. 6). At neutral pH the charge transfer is nearly eliminated and the direction of the fast photocurrent is reversed (Fig. 6; outward charge movement is positive and inward is negative). The suppressor effect of H75(57)A on W34(16)D provides evidence for the existence of a similar oligomeric interaction of wild-type BPR in living cells as is observed in the crystal structure.

A possible mechanism of the suppressor effect is suggested by consideration of a prior study of the role of His75(57) in GPR (Bergo *et al.*, 2009). In this study, spectroscopic evidence strongly indicated that His75(57) is positively charged in the dark state of proteorhodopsins and undergoes a deprotonation during the photocycle. Therefore, the W34(16)D mutation would be expected to create an Asp34(16)–His75(57) ion pair, which is likely to alter the function of His75(57), *e.g.* by preventing, altering or redirecting the His-deprotonation reaction. The presence of His75(57) is not essential for outward proton transport in GPR (Bergo *et al.*, 2009). Similarly, mutation of His75(57) to Ala in BPR accelerates the fast photocurrents but without significant changes in overall charge transfer (Fig. 6). Notably, the H75(57)A mutation completely eliminates the dramatic effect of the W34(16)D mutation (Fig. 6), as would be expected as discussed above if the W34(16)D effects were mediated through interaction with the His75(57) residue.

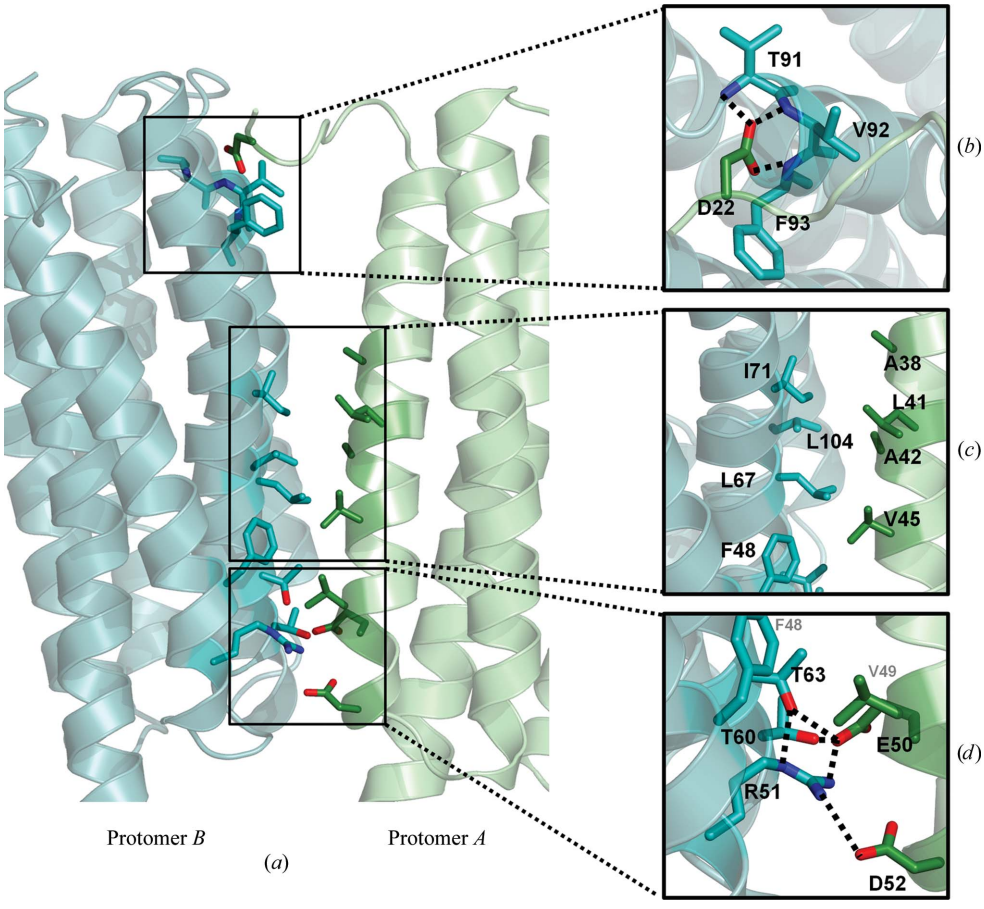

Figure 3
Protomer interface of *HOT75*BPR. (*a*) The interface between neighboring promoters (chains *A* and *B*) consists of distinct regions of interaction. At the periplasmic face, an eight-residue extension of the N-terminus of promoter *A* interacts with the neighboring promoter *B*. A more detailed look (*b*) reveals hydrogen bonding between the side chain of Asp22 (absent in *Med12*BPR), located on the N-terminal extension, and the main-chain amide N atoms of Tyr91(73), Val92(74) and Phe93(75) of the adjacent protomer. *Med12*BPR lacks this N-terminal extension and this interaction is unique to *HOT75*BPR. Interactions in the membrane-embedded region (*c*) mainly consist of a patch of hydrophobic residues. A network of salt bridges and hydrogen bonds between a polar patch of residues is found near the cytosolic face of the protomers. This network consists of five residues (*d*): Glu50(32) and Asp52(35) of protomer *A* and Arg51(33), Thr60(42) and Thr63(45) of protomer *B*. Similar hydrophobic interactions in the membrane-embedded region and salt bridges near the cytosolic face of the protein are observed in the *Med12*BPR crystal structure (not shown), but the extended N-terminus is absent, resulting in no interaction analogous to that depicted in (*b*). The figures were generated with *PyMOL*.

3.4. Structure comparison with other microbial rhodopsins reveals a different proton-translocation pathway

There are some remarkable differences between the proteorhodopsin crystal structures and other reported structures of microbial rhodopsins, such as sensory rhodopsin II (Luecke *et al.*, 2001), xanthorhodopsin (Luecke *et al.*, 2008) and bacteriorhodopsin (Luecke *et al.*, 1999). Based on the main-chain root-mean-square deviation (r.m.s.d.), *HOT75*BPR and *Med12*BPR are more closely related to BR than to XR (Fig. 7). The *HOT75*BPR mutants have an r.m.s.d. of about 1.8 Å when aligned with BR and 2.4 Å when aligned with XR. *Med12*BPR has an r.m.s.d. of 1.5 Å when aligned with BR and an r.m.s.d. of about 2.1 Å when aligned with XR. The sequence identities of BPR *versus* BR and BPR *versus* XR do not

vary greatly (*Med12*BPR has a sequence identity of 28.4% to BR and 29.8% to XR; *HOT75*BPR has a sequence identity of 26.1% to BR and 26.6% to XR).

Considerable differences from other microbial rhodopsins are the tilt and rotation of helices owing to the different length and arrangement of the loop region. Interhelical loops in PR differ from those of other microbial rhodopsins, especially the loop region between helices *B* and *C*. This loop is much shorter than those of all other microbial rhodopsins (Fig. 8) owing to the elongation of the C-terminus of helix *B* by four residues and is lacking the β-strands that are present in the structures of other microbial rhodopsins. BR has an antiparallel β-sheet which shields the proton-release region from the extracellular side, while BPR has a relatively short loop that leaves this region exposed (Fig. 8*a*). The *B*–*C* interhelical segment of XR also consists of an antiparallel β-sheet, as in BR, but this region is flipped towards the N-terminus, resulting in a large cavity near the proton-release group (Fig. 8*b*). A similar cavity exists in *Med12*BPR and *HOT75*BPR, but to a lesser degree because the displacement of the *B*–*C* and *F*–*G* interhelical segments is not as large. This region has direct access to the extracellular side because it is not blocked by an extended *B*–*C* interhelical segment (Fig. 8*c*).

At the extracellular side, there is no intramolecular interaction between the interhelical loops in BPR, a characteristic that is also seen in BR and XR. Helix *A* of both PR variants is about the same length as helix *A* of BR. XR has an extra coil of about four residues on the N-terminal side of helix *A*. Additionally, the tilt of helix *A* in both BPR variants is similar to the tilt observed in BR but not that in XR. Helix *G* of *Med12*BPR is about three residues longer than the equivalent helix in BR (it may be longer, but there is a lack of electron density to support this). Helix *G* of *HOT75*BPR is similar in length to that in XR and therefore significantly longer than helix *G* of BR. However, helix *G* in both BPR variants has a tilt similar to that in BR but not that in XR.

As evident in the *Med12*BPR crystal structure, the retinal-binding pocket shares similarities with other microbial rhodopsins, but structural comparison reveals a significantly different position of the retinal molecule (Fig. 9*a*). A greater tilt of the N-terminus of helix *G* relative to helices *C* and *D* causes the side chain of Asp227(209), which forms a hydrogen bond to Tyr200(183), to protrude further into the retinal-binding pocket, and the phenyl ring of Tyr200(183), which is parallel to the plane of the retinal molecule, is also shifted more into the plane of the retinal polyene chain. As a result, the retinal tail deviates from other rhodopsins and is pushed more towards helix *C* in the crystal structure, while

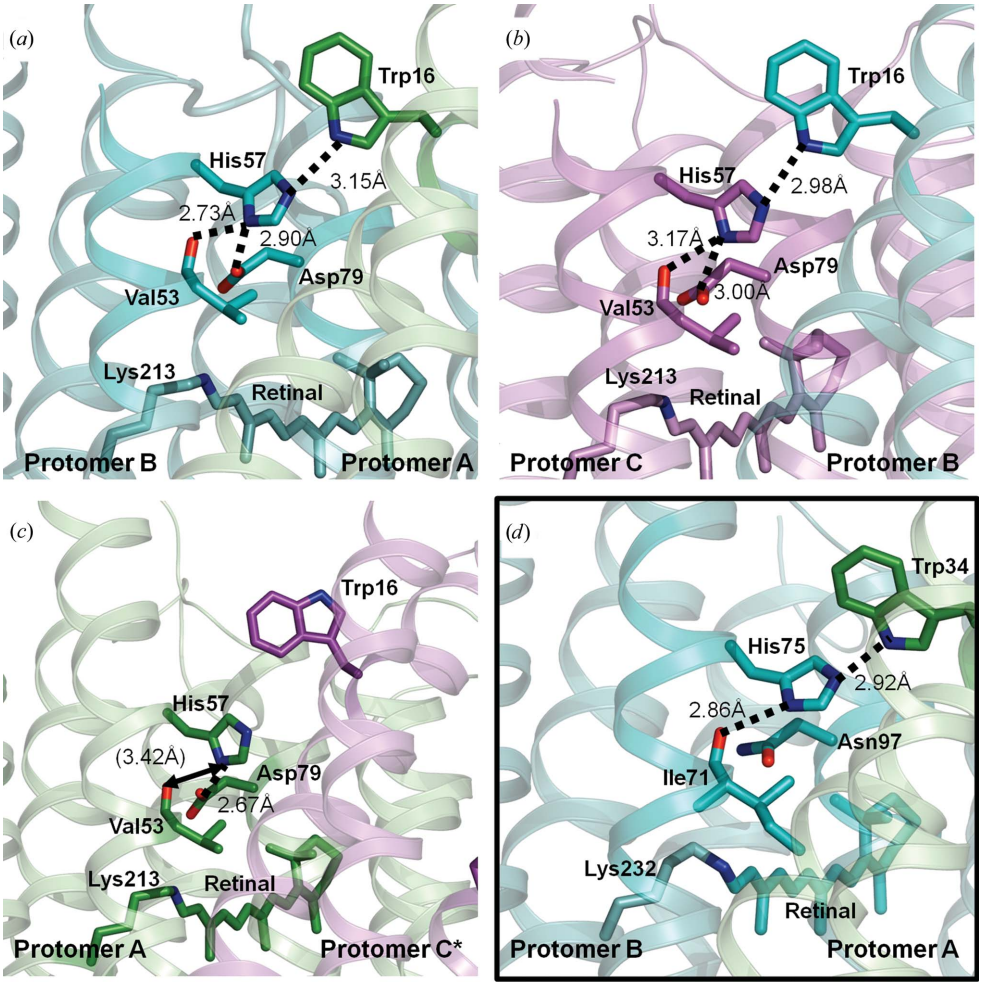

Figure 4
Coordination of His75(57) and Trp34(16) in BPR variants. (*a*) Protomer *B* of *Med12*BPR with a focus on His75(57). His75(57) donates a hydrogen bond to Asp97(79) (2.90 Å) and also to the carbonyl of Val53 (2.73 Å; Ile71 in *HOT75*BPR). In addition, its NE2 atom accepts a weak hydrogen bond (3.15 Å) from Trp34(16) of the neighboring chain *A*. (*b*) Protomer *C* of *Med12*BPR with a focus on His75(57). Hydrogen bonding is similar to that seen in protomer *B*, with His75(57) accepting a hydrogen bond from Trp34(16) of a neighboring protomer *B* (2.98 Å) and donating to the side-chain carbonyl of Val53 (3.17 Å) and Asp97(79) (3.00 Å). (*c*) Interaction of His75(57) in native BPR protomer *A* with neighboring residues. His75(57) forms a 2.67 Å hydrogen bond to Asp97(79), but the NE2 atom of the histidine is left without an ordered interaction partner as a result of Trp34(16) of a neighboring chain having its indole ring flipped such that NE1 is facing away from His75(57). (*d*) View of the region surrounding His75(57) in *HOT75*BPR D97N chain *B*. His75(57) accepts a hydrogen bond from Trp34(16) of the neighboring protomer *A* with a distance of 2.92 Å and donates a hydrogen bond to the carbonyl of Ile71 (Val53 in *Med12*BPR) (2.86 Å). Comparable interactions and distances are found in all remaining pairs of protomers in the *HOT75*BPR D97N and D97N/Q105L mutants. The figures were generated with *PyMOL*.

the retinal ring is located in a similar position as reported for other microbial rhodopsins. There is a clear shift of the retinal polyene chain and Tyr200(183) in BPR when compared with the other structures. The largest distance between the BR and BPR retinal molecules is found between the C14 atoms (1.11 Å). Similarly, there is a distance of 1.22 Å between the hydroxyl groups of Tyr185 in BR and Tyr200(183) in BPR. The position of the conserved Trp98(80) (86 in BR) shows little variation between the two structures (Fig. 9*b*).

3.5. Ion translocation

A key difference between both BPR structures and BR is the absence of water 402, which acts as a hydrogen-bond acceptor to the Schiff base. The CG atom of Asp227(209) (Asp212 in BR) is moved about 1.1 Å towards the Schiff base in relation to BR. However, the C14 atom of retinal in BPR is also shifted 1.1 Å away from the same atom in BR, so this shift represents a general movement in the environment and not a decreased distance between the Schiff base and Asp227(209), which makes it unlikely that this residue can accept a proton in a more direct mechanism that does not involve water clusters. Nonetheless, in protomer *A* of *Med12*BPR Asp227(209) (Asp212 in BR) comes within hydrogen-bonding distance of the Schiff base while being coordinated by the nearby Tyr76(58) and Tyr200(183) (Fig. 10*a*). Asp227(209) also makes a direct hydrogen bond to Arg94(76) (Arg82 in BR), which is instead coordinated by structural waters in BR. Kinetic measurements of proton transfer from the Schiff base in wild-type and mutant BPRs indicated that unlike in BR, there are two alternative proton acceptors in BPR: Asp97(79), the residue corresponding to the acceptor in BR, and another residue of similar pK_a, possibly Asp227(209) (Sineshchekov & Spudich, 2004).

However, in protomers *B* and *C* of *Med12*BPR, Asp227(209) is no longer within hydrogen-bonding distance of the Schiff base, which itself does not have a clear hydrogen-bond acceptor (Figs. 10*b* and 10*c*). Coordination of Asp227(209) is maintained by the hydroxyl groups of Tyr76(58) and Tyr200(183) in both protomers, but no clear interaction exists with Arg94(76) in protomer *B*. Additionally, in protomer *C* the carboxyl group of Asp227(209) is also within distance to accept a hydrogen bond from the indole N atom of Trp98(80). Three structural waters are critical for coordination in BR (Fig. 10*d*), yet no electron density exists to support their involvement in BPR. Hydrogen bonds connect key atoms involved in the BR mechanism, including Arg82, Asp85 and the retinal Schiff base. Asp85 acts as the proton acceptor in the first part of the BR photocycle, yet the homologous residue in BPR, Asp97(79), does not appear to be within hydrogen-bonding distance of the region. This residue is severely rotated in *Med12*BPR and is in a similar position to Asp96 of XR.

*Med12*BPR has an alanine (Ala47; Ser65 in *HOT75*BPR) in place of Thr46 in BR, which is thought to be involved in the initial translocation of a proton from the intracellular side into the protein (Rouhani *et al.*, 2001). Glu108(90) (Asp96 in BR) of *Med12*BPR forms a hydrogen bond to the main-chain carbonyl of Ser61(43) (2.91 Å), which itself is within hydrogen-bonding distance (3.07 Å) of the main-chain N atom

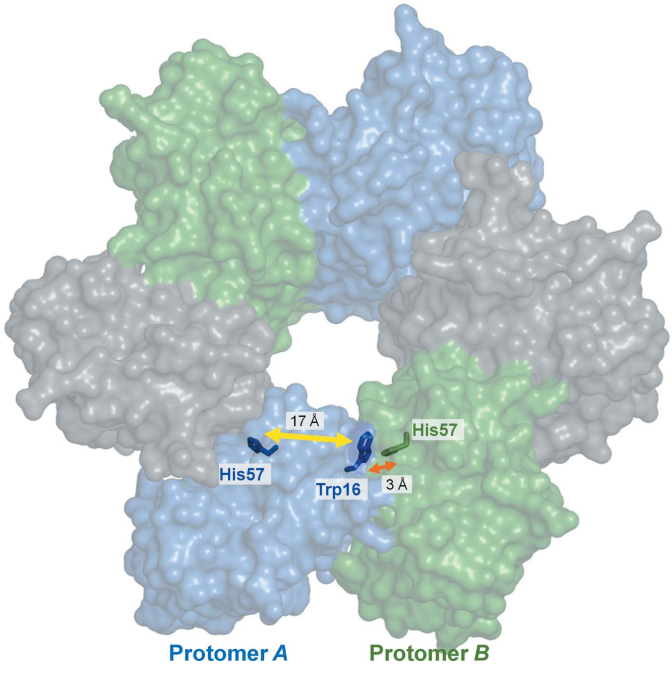

Figure 5
Intra-protomer and inter-protomer His75(57)–Trp34(16) distances in the *Med12*BPR hexamer. The distance between His75(57) of one protomer and Trp34(16) of a neighboring protomer is significantly shorter than the distance to Trp34(16) in the same protomer. This figure was generated with *VMD* (Humphrey *et al.*, 1996).

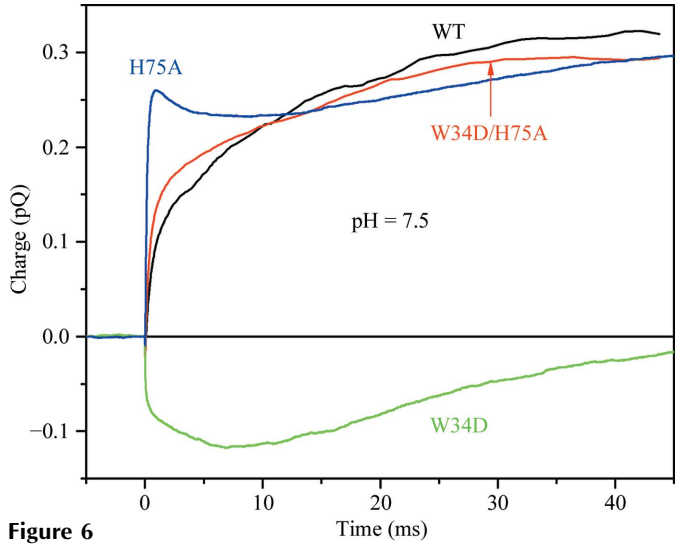

Figure 6
Photocurrents produced by *HOT75*BPR and mutants. Light-induced intramolecular charge movement in suspensions of intact *E. coli* cells was measured following the photoelectric method described in Sineshchekov & Spudich (2004). A 532 nm 6 ns flash from an Nd:YAG Surelite I laser (Continuum, Santa Clara, California, USA) was delivered at time 0 and the electrical currents were measured. Charge transfer was calculated as an integral of the photocurrent. Outward charge movement (defined as the direction from the cytoplasm to the periplasm) is positive and inward is negative. The 'WT' trace in red is the photocurrent from *E. coli* expressing wild-type *HOT75*BPR and the green, blue and black traces are from *E. coli* expressing *HOT75*BPR carrying the mutations indicated.

of Ala47 (Ser65 in *HOT75*BPR). This may serve as a path for proton translocation from the cytoplasm to the Schiff-base donor.

3.6. The putative proton-release region in proteorhodopsin differs from that in bacteriorhodopsin

In BR, a pair of glutamates and several waters on the extracellular side of Arg82 play a crucial role during proton release (Spassov *et al.*, 2001). In proteorhodopsins, there is a conserved aspartate [Asp212(194)] in the *F*–*G* loop, but it is located more than 21 Å from the conserved Arg94(76) in the *Med12*BPR structure, so this residue is unlikely to accept the proton from protonated Arg94(76). BPR has both glutamic acids replaced with a tyrosine and a leucine, respectively. However, a new glutamic acid, Glu142(124), resides in this region (Fig. 10*a*). It is in a similar position to Glu141 in XR, and the distance between Arg94(76) CZ and Glu142(124) CD is 8.37 Å. Additionally, Arg94(76) is in a similar conformation to Arg82 in BR, but shifted such that the Arg76 CZ–Arg82 CZ distance is 1.11 Å. Once again, this is a reflection of a general shift in this region.

In both BPR structures, instead of a pair of glutamates as in BR, Glu142(124) is situated in a region similar to the Glu194 proton-release group in BR and is coordinated *via* hydrogen bonds to three neighboring tyrosine residues [Tyr95(77), Tyr208(191) and Tyr223(205); Fig. 11*b*]. The glutamate is connected to Arg94(76) (Arg82 in BR) *via* a network of hydrogen bonds involving two waters (Wat403 and Wat405), Thr91(73) and Asn220(202) (Fig. 11*c*). A key difference between BR and BPR is the inclusion of a second proton-release group in BR, Glu204, and the absence of tyrosine residues involved in coordination (Fig. 11*d*), yet a similar network is formed between Arg82 and Glu194 *via* two water molecules. We aligned 3229 PR sequences from NCBI and found that Glu142(124) is nearly 100% conserved, with only ten of these lacking a glutamate at the corresponding position, which implies an important role of Glu142(124) throughout the family.

Although the structural arrangement is different, mutation of Arg94(76) to other residues abolished the proton-pumping function (unpublished data), suggesting that the translocation of protons may occur through the aqueous network rather than the movement of a side chain of residue 94(76), and

	Sequence identity (%)												
	*Med12*BPR	*HOT75*BPR D97N	*HOT75*BPR D97N/Q105L	GPR (2l6x)	BR (1cw3)	HR (1e12)	SRII (1jgj)	ASR (1xio)	XR (3ddl)	AR2 (3am6)	aR-1 (1uaz)	ChR (3ug9)	SRII (2ksy)
*Med12*BPR		61	62	55	28	15	25	21	30	22	25	17	24
*HOT75*BPR D97N	0.76		94	66	26	17	28	17	27	22	23	16	26
*HOT75*BPR D97N/Q105L	0.67	0.44		70	27	18	29	19	27	23	26	16	27
GPR (2l6x)	3.22	3.17	3.24		19	15	21	15	18	21	19	13	24
BR (1cw3)	1.48	1.60	1.75	3.42		34	29	31	24	32	61	18	29
HR (1e12)	1.77	1.88	1.94	3.62	1.37		28	27	19	24	35	18	27
SRII (1jgj)	1.55	1.80	1.98	3.52	1.06	1.51		30	20	29	31	16	98
ASR (1xio)	1.82	2.14	1.92	3.47	1.35	1.21	1.26		21	27	34	20	28
XR (3ddl)	2.09	2.21	2.35	3.89	1.93	2.12	2.03	2.03		19	27	17	19
AR2 (3am6)	2.07	1.88	1.90	3.74	1.24	1.48	1.31	1.43	2.16		30	22	28
aR-1 (1uaz)	1.60	1.72	1.98	3.60	0.80	1.24	1.07	1.32	2.02	1.27		23	31
ChR (3ug9)	2.25	2.22	2.42	3.65	2.18	2.41	2.60	2.30	1.99	2.11	2.21		17
SRII (ssNMR) (2ksy)	1.80	1.93	1.93	3.62	1.38	1.51	1.24	1.62	2.33	1.78	1.27	2.36	

Figure 7
Root-mean-square deviation (r.m.s.d.; Å) and sequence identity (%) between pairs of microbial rhodopsins. Values were calculated using *PDBeFold* (Krissinel & Henrick, 2004) using C^{α} atoms for superposition. R.m.s.d. and sequence-identity values are reported for chain pairs with the highest *Q*-score, which is based on both r.m.s.d. and number of aligned residues.

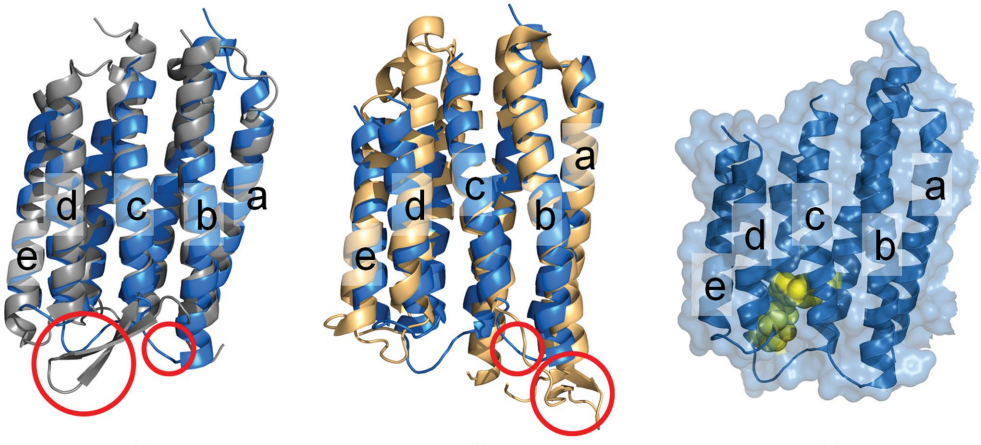

(*a*) (*b*) (*c*)

Figure 8
Comparison of *B*–*C* interhelical segments in proteorhodopsin, bacteriorhodopsin and xanthorhodopsin. (*a*) Superposition of the BR protomer (gray; PDB entry 1c3w; Luecke *et al.*, 1999) onto *Med12*BPR protomer *A* (blue; r.m.s.d. = 1.48 Å). The *B*–*C* interhelical segment of each protein is circled. BR has an antiparallel β-sheet which shields the proton-release region from the extracellular side, while BPR has a relatively short loop that leaves this region exposed. (*b*) Superposition of the XR protomer (light orange; PDB entry 3ddl; Luecke *et al.*, 2008) onto *Med12*BPR protomer *A* (blue; r.m.s.d. = 1.98 Å). The *B*–*C* interhelical segment of XR also consists of an antiparallel β-sheet, as in BR, but this region is flipped towards the N-terminus, resulting in a large cavity near the proton-release group. A similar cavity exists in BPR but to a lesser degree because the displacement of the *B*–*C* and *F*–*G* interhelical segments is not as large. (*c*) Space-filling model of *Med12*BPR protomer *A* with the seven helices highlighted. The putative proton-release group of Glu142(124), Tyr95(77), Tyr208(191) and Tyr223(205) is displayed as a space-filling model colored yellow. This region has direct access to the extracellular side because it is not blocked by an extended *B*–*C* interhelical segment. The figures were generated with *PyMOL*.

that Arg94(76) is critical for the process. Mutants of Asn221(202), Asn225(206) and Tyr76(58) all impaired the proton-translocation activity of PR, with the Y76(58)F single mutant losing 95% of activity (unpublished data).

3.7. Interaction of Gln105(87) of native blue-light-absorbing proteorhodopsin with its environment

Gln105(87) in *Med12*BPR, which is responsible for spectral tuning to blue wavelengths, is involved in a network mediated by Wat503, which forms hydrogen bonds with the Gln105(87) side chain and the main-chain carbonyl of Asn230(212) in protomer *A* (Fig. 12*a*). The introduction of a second water is seen in protomer *B* of *Med12*BPR between the side chains of Gln105(87) and Trp197(180), which joins the two residues *via* hydrogen bonds, and in this conformation Gln105(87) is within distance to hydrogen bond directly to the main-chain carbonyl of Asn230(212) without a structural water to act as an intermediate (Fig. 12*b*). Unlike protomers *A* and *B* of *Med12*BPR, there is no electron density to suggest the presence of structural waters in this region in protomer *C*. However, Gln105(87) is within direct hydrogen-bonding distance of Trp197(180) and the main-chain carbonyl of Asn230(212).

Additionally, the side chain of Asn230(212) is able to interact with Trp197(180) (Fig. 12*c*). Hydrogen bonding was not observed in either the D97N BPR mutant or the D97N/Q105L double mutant of *HOT75*BPR. Bacteriorhodopsin contains a leucine in place of a glutamine, eliminating any hydrogen bonding involving this residue. Additionally, Asn230(212) is Ala215 in BR, preventing any additional hydrogen bonds involving the side chain. The main-chain carbonyl of Ala215 is within hydrogen-bonding distance of Wat501, which in turn forms a hydrogen bond to Trp182 (Trp197/180 in native BPR; Fig. 12*d*). Wat501 has a *B* factor of 56 Å^2 in BPR, which is higher than the other waters in the molecule. Additionally, Wat501 is only observed in one of the three protomers in the asymmetric unit. Therefore, this water molecule may play only a minor role in BPR.

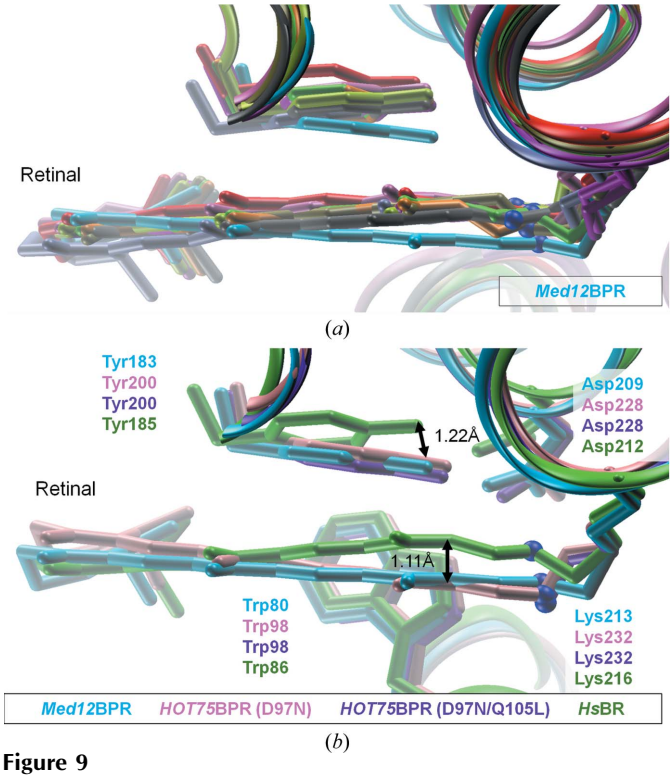

Figure 9
Overlay of the retinal Schiff base and the surrounding region of several microbial rhodopsin structures. (*a*) Several microbial rhodopsin crystal structures (PDB entries 1jgj, sensory rhodopsin II; 1c3w, native bacteriorhodopsin; 1c8r, BR D96N state; 1c8s, BR D96N late M state intermediate; 3t45, BR A215T mutant; 1jv6, BR D85S/F219L double mutant; 1jv7, BR O-like intermediate state of D85S mutant; 1ei2, halorhodopsin; 1xio, *Anabaena* sensory rhodopsin; 3ddl, xanthorhodopsin) were superimposed onto the crystal structure of *Med12*BPR protomer *A*. There is a clear shift of the retinal polyene chain and Tyr200(183) in BPR when compared with the other structures. As there is little structural variance in this region between the three protomers of *Med12*BPR, only one chain is shown for simplicity. (*b*) Superimposition of native bacteriorhodopsin, *HOT75*BPR D97N protomer *A* and *HOT75*BPR D97N/Q105L protomer *A* onto the crystal structure of *Med12*BPR protomer *A*. The retinal and tyrosine shift seen in (*a*) is consistent amongst all three variants of BPR. The Schiff-base N atom is represented as a blue sphere for reference. The figures were generated with *PyMOL*.

3.8. Comparison to the solution NMR structure of a GPR

Our crystal structures are in agreement with the general topology of the GPR solution NMR structure published by Reckel *et al.* (2011), namely seven transmembrane helices with short loops and the absence of the antiparallel β-sheet observed between helices *B* and *C* in other microbial rhodopsins, but severe deviations exist at the atomic level. However, superimposition of our crystal structures onto the solution NMR model yields at best a C^{α} r.m.s.d. of over 3.0 Å (Fig. 7), despite a relatively high number of aligned residues and sequence identities of 55% or more between the variants.

With respect to the *B*–*C* β-turn described to be formed by residues Gly87(69)–Pro90(72) in the NMR structure, our crystal structures also show this feature but with a notable difference. The $n + 4$ motif for a β-turn is observed in the range Trp83(65)–Gly87(69) (Trp83 O–Gly87 N distance of 2.76 Å) in *HOT75*BPR and also for the homologous *Med12*BPR residues Trp65–Gly69 (Trp65 N–Gly69 O distance of 2.96 Å). Pro90(72) is already part of helix *C*. In the NMR structure, the loop between helices *D* and *E* was found to be longer than suggested by secondary-structure prediction programs, but it is one of the shortest loops in *Med12*BPR (Ala125–Asp129) as well as in *HOT75*BPR (Gly144–Pro147), which is in agreement with the prediction. In contrast, the loop region connecting helices *E* and *F* in the GPR NMR structure is shorter than predicted, as residues Glu170–Asn176 form a helical extension (*E*′) of helix *E*. Helix *E*′ is connected to helix *E* through a slight helical distortion at Gly169. This is also true in *Hot75*BPR (only protomers *B* and *C* have sufficient density in this region for a full model). The helical distortion is visible at Gly196. This observation is inconclusive for *Med12*BPR because the region is disordered in all three chains. In both BPR crystal structures and the GPR NMR structure, helix *E* has approximately the same length as its neighboring helix *D*

and is thus significantly shorter than the other five helices. Additionally, the kink in helix *G* at residue Asn230(212), which is the result of the π-bulge previously observed in other microbial retinal-binding proteins (Cartailler & Luecke, 2004), is found in both variants of BPR.

Reckel *et al.* (2011) measured that the CD1 methyl group of Leu105 is one of two methyl groups showing an NOE to the C20 methyl group of retinal. This residue is a key determinant of the spectral properties of the two main variants of PR, and the NMR structure reveals its close position to the Schiff-base retinal. In the *HOT75*BPR D97N/Q105L structure the Leu105 CG–RET C20 distance is 4.38 Å and the Leu105 CG–Lys232 NZ distance is 5.95 Å. These distances are 5.25 and 6.11 Å, respectively, in BR. C20 is the nearest atom of retinal to Leu105.

We find that not all of the distance restraints used to arrive at the NMR structure are in agreement with our BPR structures. In particular, the side-chain atoms of Asp97(79) and Asp227(209) were given an upper distance limit of 5 Å to the Schiff base. It is not evident that either Asp97(79) or its mutated equivalent Asn97 are within 5 Å of the Schiff base. For *Med12*BPR, we find that the distances between three atoms of Asp97(79) and the Schiff-base N atom are outside this restraint (CB, 6.07 Å; CG, 5.10 Å; OD1, 5.66 Å). The same three atoms are more than 5 Å away from the Schiff base in *HOT75*BPR. A stronger case could be made for Asp227(209),

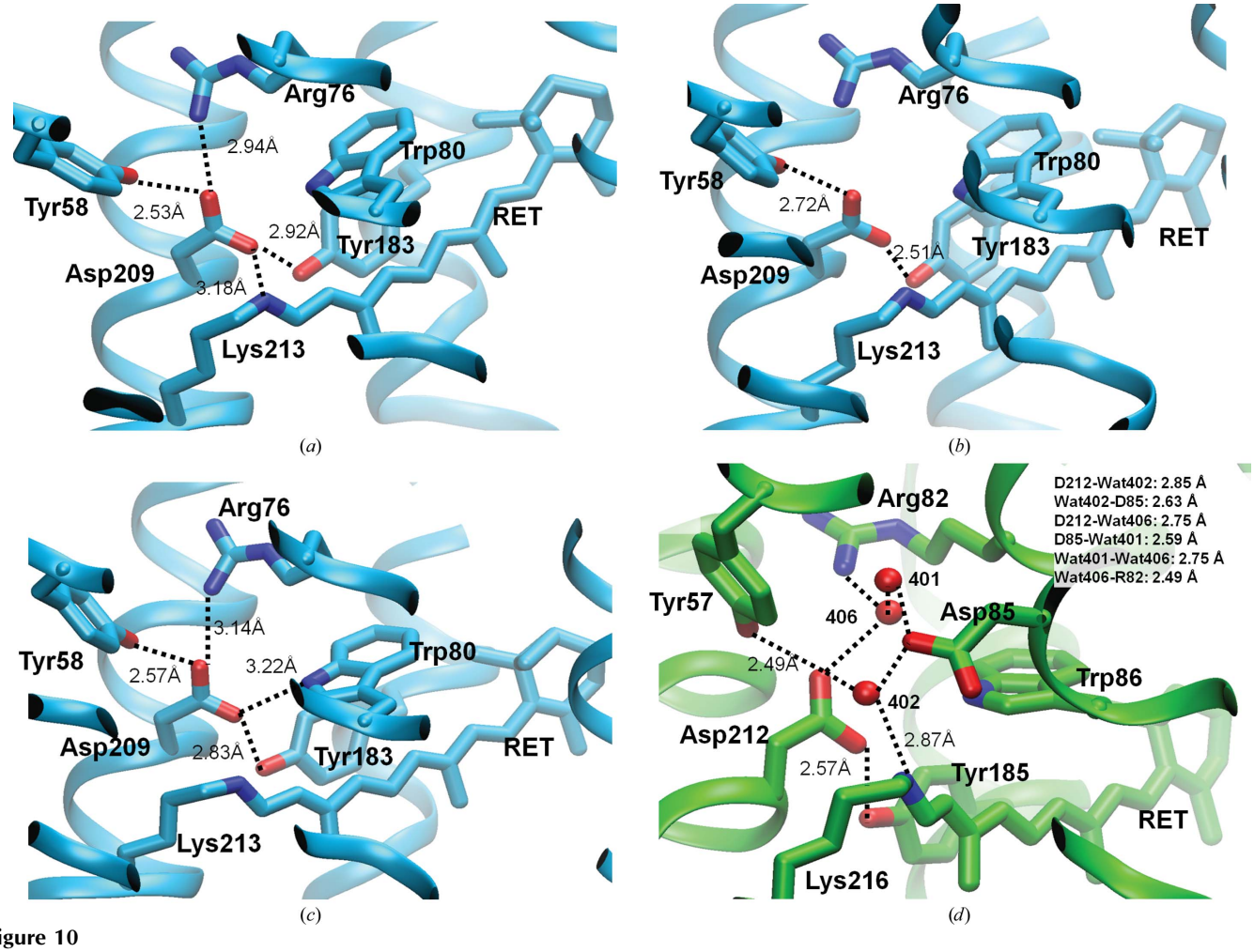

Figure 10
Comparison of the Schiff-base regions of BPR and BR. (*a*) View of the Schiff-base region of *Med12*BPR protomer *A*. A key difference from BR is the absence of water 402, which acts as a hydrogen-bond acceptor for the Schiff base. Instead, Asp227 (209; Asp212 in BR) comes within hydrogen-bonding distance of the Schiff base, while being coordinated by the nearby Tyr76(58) and Tyr200(183). Asp227(209) also makes a direct hydrogen bond to Arg94(76; Arg82 in BR), which is instead coordinated by structural waters in bacteriorhodopsin. (*b*) The Schiff-base region of *Med12*BPR protomer *B*. Asp227(209) is no longer within hydrogen-bonding distance of the Schiff base, which itself does not have a clear hydrogen-bond acceptor. Coordination of Asp227(209) is maintained by the hydroxyl groups of Tyr76(58) and Tyr200(183), but no clear interaction exists with Arg94(76). (*c*) The Schiff-base region of *Med12*BPR protomer *C*. As for protomer *B*, the Schiff base of chain *C* does not have a clear hydrogen-bond acceptor. Asp227(209) continues to be coordinated by Tyr76(58) and Tyr200(183), and a direct hydrogen bond to Arg94(76) is re-established. In addition, the carboxyl group of Asp227(209) is also within distance to accept a hydrogen-bond from the indole N atom of Trp98(80). (*d*) The complex hydrogen-bonding network near the Schiff-base region of native bacteriorhodopsin. Three structural waters are critical for coordination in BR, yet no electron density exists to support their presence in BPR. Hydrogen bonds connect key atoms involved in the BR mechanism, including Arg82, Asp85 and the retinal Schiff base. Asp85 acts as the proton acceptor during the early part of the BR cycle, yet the homologous residue in BPR, Asp97(79), is not within hydrogen-bonding distance of this region. The figures were generated with *PyMOL*.

as all of the side-chain atoms are within the restraint distance in *Med12*BPR but two are outside of the range in *HOT75*BPR. The NMR restraints may be artificially pulling Asp97(79) and Asp227(209) closer to the Schiff base than they appear in the protein. Another restraint with an upper limit of 7 Å was placed on the distance between Tyr200(183) and the ring structure of the retinal. While the backbone atoms of Tyr200(183) are within the 7 Å limit in all three crystal structures, atoms CE1, CE2, CZ and OH of the side chain are at distances greater than 7 Å (the tyrosine ring points 180° away from the retinal ring).

3.9. Comparison of PR and BR oligomer interfaces

The oligomerization states of the two variants of PR differ not only from each other (hexamer *versus* pentamer) but also from that of BR (trimer). Based on their arrangement in the type I membrane-protein crystal and previously published results suggesting that PR forms a trimer or hexamer, it is likely that the arrangements seen in the crystal structures are physiologically relevant. The surface area of the BR trimer interface was calculated to be 710 Å^2, which increases to 774 Å^2 for the *Med12*BPR hexamer and 863 Å^2 for the *HOT75*BPR pentamer, with twice the respective area buried for each protomer that is part of a $C_3/C_5/C_6$ ring. Analysis comparing the three assemblies reveals that while there is some overlap between the interfaces, there are clear differences between BR and the PRs and even between the two PR variants (Fig. 13). In fact, the interface regions involve different helices (Fig. 14). In BR, several interactions occur along the entire face of helix *D*, a section of helix *B* and parts

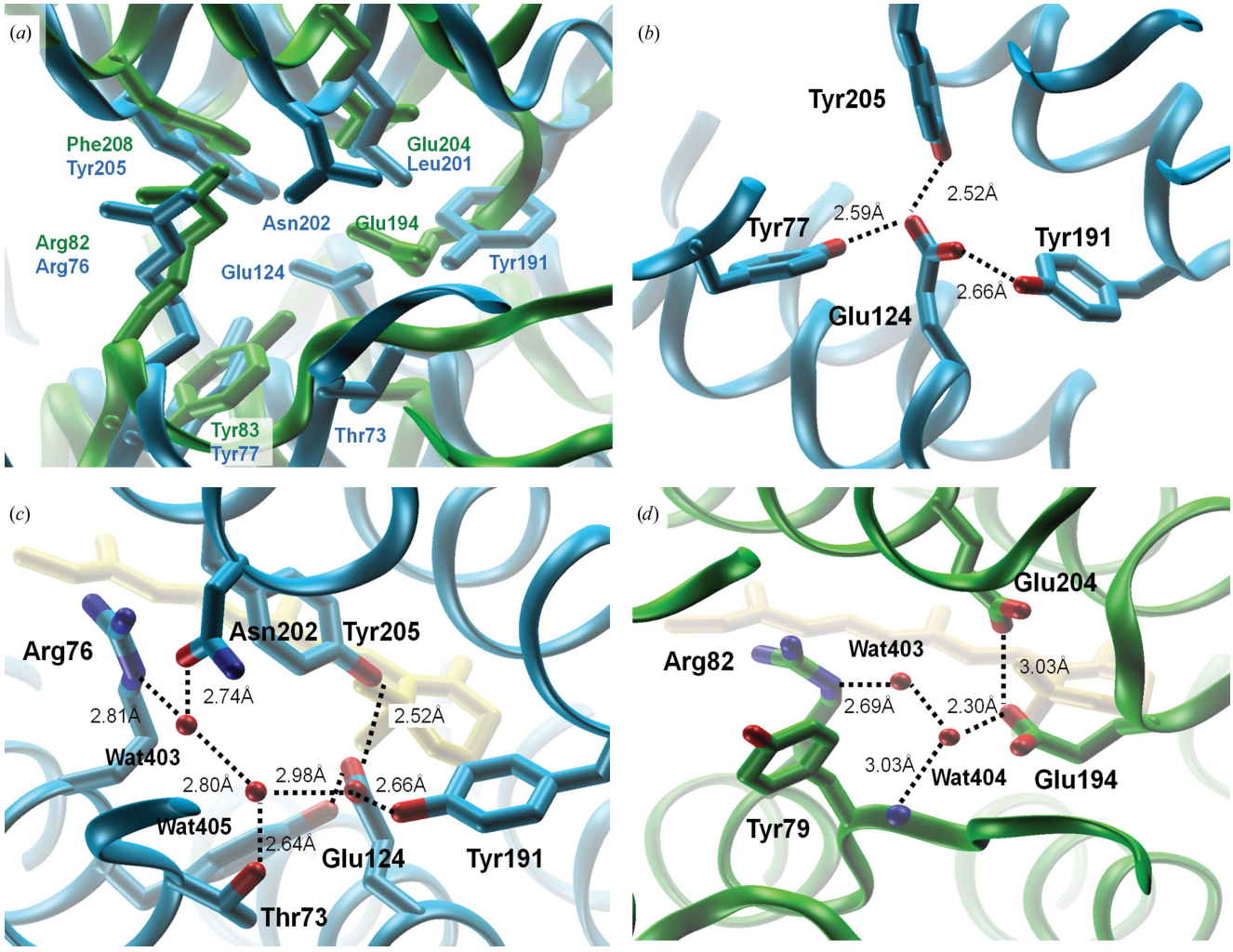

Figure 11
Putative proton-release region in BPR with comparison to BR. (*a*) Superimposition of the proton-release regions of *Med12*BPR protomer *A* (colored blue) and BR (colored green), with key residues labeled. It is noteworthy that Glu194 and Glu204 of BR are mutated to Tyr208(191) and Leu219(201), respectively, in BPR, yet Glu142(124; Ala126 in BR) is able to take the place of the mutated residues and involve itself in the hydrogen-bonding network. (*b*) Glu142(124) in *Med12*BPR protomer *A* is coordinated *via* hydrogen bonds to three neighboring tyrosine residues. The residue is situated in a region similar to the Glu194 proton-release group in bacteriorhodopsin. (*c*) A constituent of the putative proton-release group in *Med12*BPR protomer *A*, Glu142(124), is involved in a network of hydrogen bonds to key residues and structural waters. This network extends to Arg94(76) (Arg82 in BR), a key residue in spectral tuning that is possibly involved in the proton-pumping mechanism. (*d*) Bacteriorhodopsin forms a similar hydrogen-bond network involving Glu194, Glu204, Arg82 and two structural waters. A key difference from *Med12*BPR is the inclusion of a second carboxylate, Glu204, and the absence of tyrosine residues involved in coordination. The figures were generated with *PyMOL*.

of helix *E* (Fig. 14*b*). In both variants of PR, helix *A* is heavily involved in the interface, along with helix *C*. *Med12*BPR and *HOT75*BPR have many interface regions in common, with the main exception being the N-terminal tail preceding helix *A* that interacts with helix *B* of the neighboring protomer. Despite the different oligomeric states between BR and the two PR variants, the portion of the interface involving helices *B* and *C* has several regions that are conserved.

4. Discussion

Previous studies employing AFM on two-dimensional patches of a membrane-embedded GPR showed coexisting hexamers and pentamers (Klyszejko *et al.*, 2008), presumably the same C_6 and C_5 species reported here as high-resolution crystal structures. More recently, solution studies using SEC-LS/UV/RI, ESR spectral line-shape analysis and Overhauser DNP methods determined that the predominant species of a GPR was a hexamer with an arrangement such that the loop between helices *A* and *B* was close to the hexamer center, with a distance between spin labels on an engineered cysteine at residue 55 (Ser55 in GPR and *HOT75*BPR and Pro37 in *Med12*BPR) of about 19 Å (Stone *et al.*, 2013). This distance appears to be consistent with both of the crystal structure oligomers described here (hexamer and pentamer), in which the C^{α}–C^{α} distances for immediate neighbors of this residue are 15.8 and 14.8 Å, respectively (hexamer, *A*–*B* = 16.03 Å, *B*–*C* = 15.34 Å, *C*–*A*′ = 16.06 Å; pentamer, *A*–*B* = 14.75 Å, *B*–*C* = 14.81 Å, *C*–*D* = 14.76 Å, *D*–*E* = 14.74 Å, *E*–*A* = 14.71 Å).

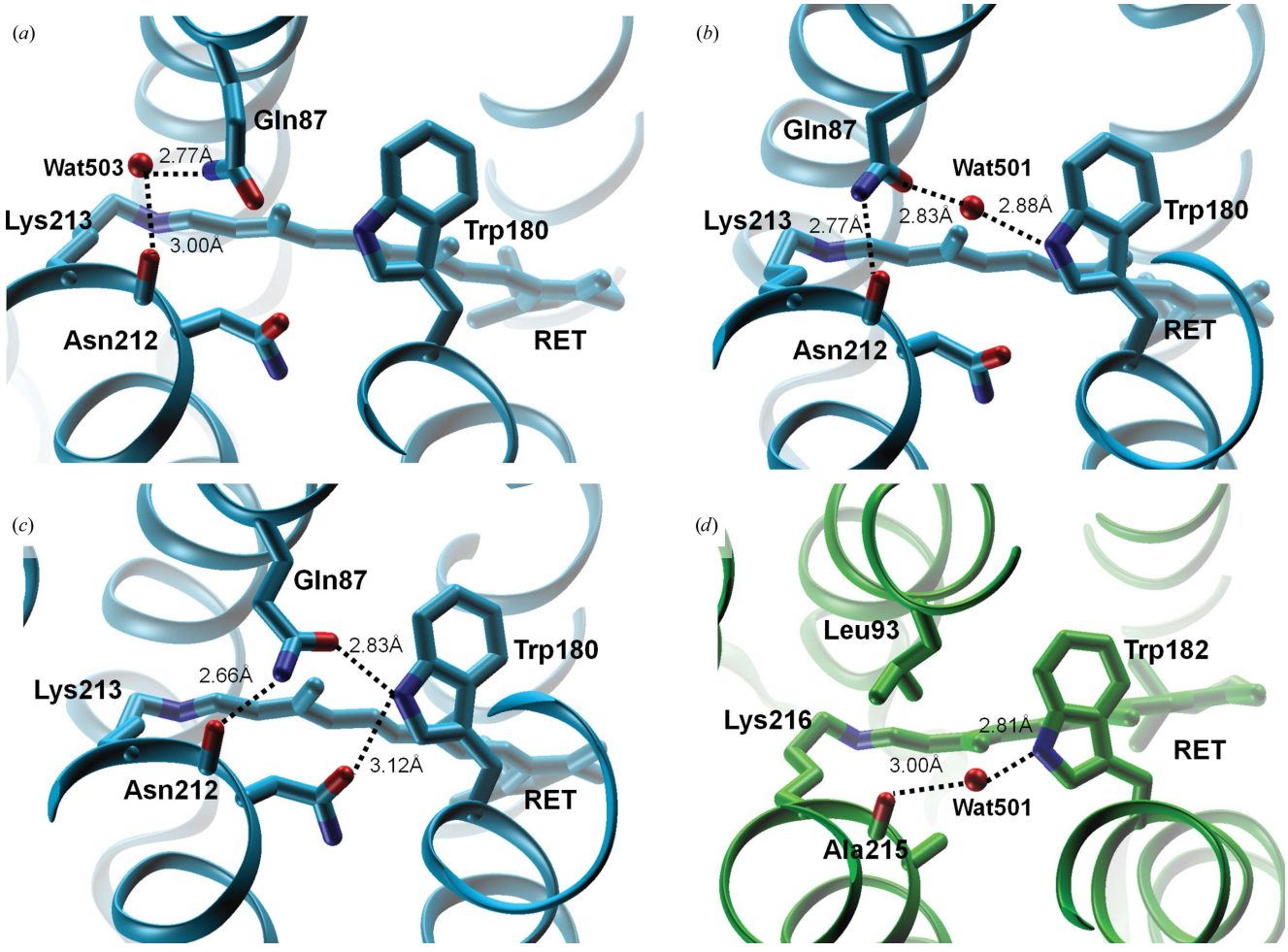

Figure 12
Interaction of Gln105(87) of BPR with its environment compared with that of BR. (*a*) Protomer *A* of *Med12*BPR. Structural water 503 is involved in hydrogen bonding between the Gln105(87) side chain and the main-chain carbonyl of Asn230(212). (*b*) Protomer *B* of *Med12*BPR. Gln105(87) is within distance to hydrogen bond directly to the main-chain carbonyl of Asn230(212) without a structural water to act as an intermediate. A structural water (501) is now positioned between Gln105(87) and Trp197(180), mediating an interaction between the two residues. (*c*) Protomer *C* of *Med12*BPR. Unlike protomers *A* and *B*, there is no electron density to suggest the presence of structural waters in this region. However, Gln105(87) is within direct hydrogen-bonding distance of Trp197(180) and the main-chain carbonyl of Asn230(212). Additionally, the side chain of Asn230(212) is able to interact with Trp197(180). Hydrogen bonding was not observed in the D97N mutant nor in the D97N/Q105L double mutant of *HOT75*BPR. (*d*) Homologous region in bacteriorhodopsin. BR contains a leucine in place of a glutamine, eliminating any hydrogen bonding involving this residue. Additionally, Asn230(212) is Ala215 in BR, preventing any additional hydrogen bonds involving the side chain. The main-chain carbonyl of Ala215 is within hydrogen-bonding distance of Wat501, which in turn forms a hydrogen bond to Trp182 (Trp197/180 in BPR). All figures were generated with *PyMOL*.

We then presented data demonstrating that oligomer formation and the resulting inter-protomer interactions strongly affect the photocycle and thus function. The cross-protomer hydrogen bond between Trp34(16) and His75(57) of a neighboring chain is a unique feature that has not been observed previously in microbial rhodopsins. His75(57) also makes a hydrogen bond to Asp97(79), the Schiff-base proton acceptor in the proton-transport process, suggesting that the Trp–His bond may influence proton transport and suggesting a possible physiological role of this inter-protomer network. These suggestions are confirmed by the effect of the mutation of Trp34(16) to Asp, which produces a His75(57)-dependent reversal of the outward proton translocation from the Schiff base to Asp97(79) in the wild type to inward transfer to the cytoplasmic side of the protein.

A possible mechanism whereby the Trp34(16)–His75(57) pair could facilitate proton transfer from the Schiff base to Asp97(79) in wild-type PR is as follows: as a result of the isomerization of the retinal, an early conformational change results in the protomer containing the His75(57) member of the hydrogen-bonded pair moving relative to the adjacent protomer containing the nearby Trp34(16). This movement shifts NE2 of His75(57) away from the nearby hydrogen-bond donor [Trp34(16)], making protonation of this N atom more favorable. In turn, ND1 is no longer protonated, raising the pK_a of

```
BR       | ---MLELL---------PTAVEGVSQAQITGRPEWIWLALGTALMGLGTLYFLVKGMGVS 35
Med12BPR| -------------------MGEILAVDDYVGISFW--L--AAAIMLASTVFFFVERSDVP 37
HOT75BPR| MGKLLLILGSAIALPSFAAAGGDLDISDTVGVSFW--L--VTAGMLAATVFFFVERDQVS 55
                                 :   : .*   *  *   :* *  .*::*:*:   *

BR       | DPDAKKFYAITTLVPAIAFTMYLSMLLGYGLTMVPFGGEQNPIYWARYADWLFTTPLLLL 95
Med12BPR| V-KWKTSLTVAGLVTGVAFWHYLYMRGV-----WIYAGETP--TVFRYIDWLITVPLQII 89
HOT75BPR| A-KWKTSLTVSGLITGIAFWHYLYMRGV-----WIDTGDTP--TVFRYIDWLLTVPLQVV 107
           . *.  ::: *: .:**  ** *            *:       ** ***:*.** ::

BR       | DLALLVDADQGT----ILALVGADGIMIGTGLVGALTKVYSYRFVWWAISTAAMLYILYV 151
Med12BPR| EFYLIIAAVTAISSAVFWKLLIASLVMLIGGFIGEAG--LGDVVVWWIVGMIAWLYIIYE 147
HOT75BPR| EFYLILAACTSVAASLFKKLLAGSLVMLGAGFAGEAG--LAPVLPAFIIGMAGWLYMIYE 165
           :: *:: *  .     :  *: .. :*:  *: *      .  .  : :.  . **::*

BR       | LFFGFTSKAE--SMRPEVASTFKVLRNVTVVLWSAYPVVWLIGSE--GAGIVPLNIETLL 207
Med12BPR| IFLGETAKANAGSGNAASQQAFNTIKWIVTVGWAIYPIGYAWGYF--GDGLNEDA-LNIV 204
HOT75BPR| LYMGEGKAAV-STASPAVNSAYNAMMMIIVVGWAIYPAGYAAGYLMGGEGVYASN-LNLI 223
           :::*    *   :      .:::.:  : .* *: **  :  *    * *:      .::

BR       | FMVLDVSAKVGFGLILLRSRAIFGEAEAPEPSAGDGAAATSD 249
Med12BPR| YNLADLINKAAFGLAIWAAAMKDKETSTSHA----------- 235
HOT75BPR| YNLADFVNKILFGLIIWNVAVKESSNA--------------- 250
           : : *.  *  *** :        .
```

Figure 13
Sequence alignment of BR, *Med12*BPR and *HOT75*BPR, with regions involved in oligomerization highlighted. Residues highlighted in blue are found on protomer *A* of each molecule and are involved in the interface with protomer *B* (residues highlighted in green). Red highlights indcate residues that form hydrogen bonds or salt bridges.

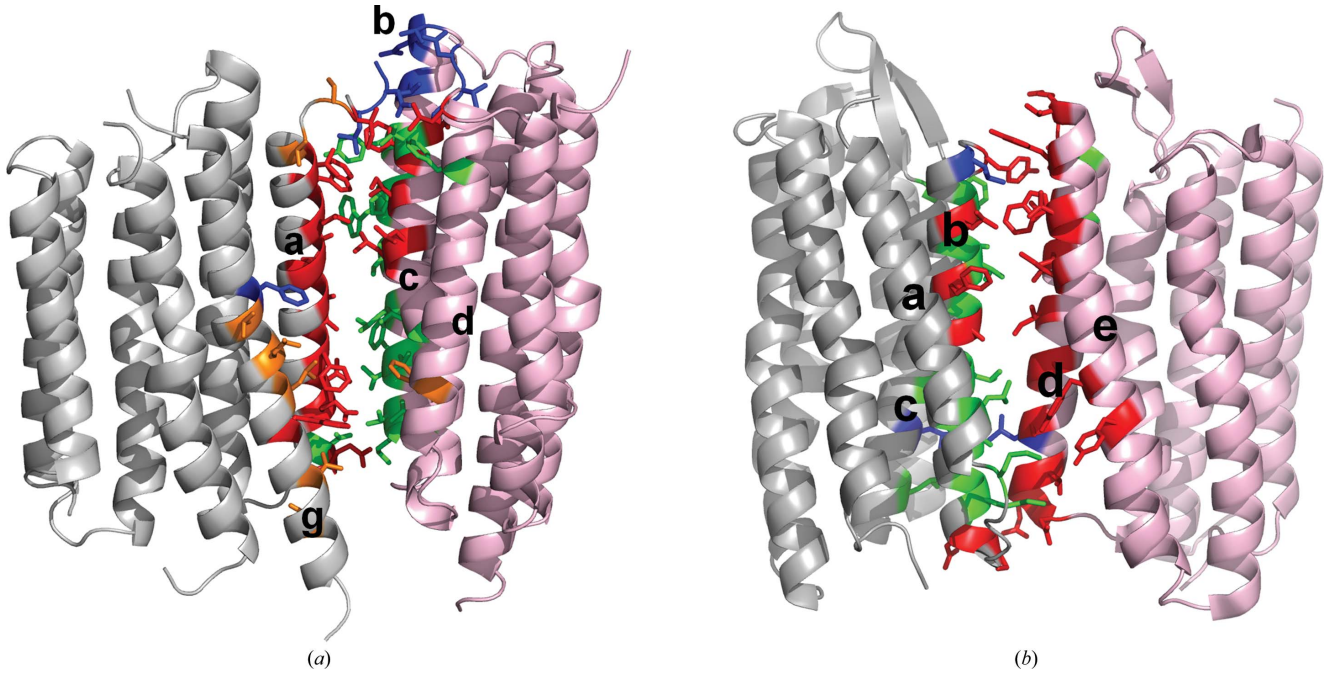

(*a*) (*b*)

Figure 14
Comparison of regions involved in BR and PR oligomerization. (*a*) Protomer interface of chains *A* (gray) and *B* (pink) of *HOT75*BPR. Residues unique to the *HOT75*BPR interface are colored blue, while residues unique to the *Med12*BPR interface are colored orange. Interfaces that are common to both variants of PR but not BR are colored red and regions common to interfaces in both PR and BR are colored green. Helices are labeled with lowercase letters. (*b*) Protomer interface of chains *A* (gray) and *B* (pink) of BR. Residues unique to the BR interface are colored red. Regions that are in common between BR and one of the two PR variants are colored blue and regions that are common to all three structures are colored green. Helices are labeled with lowercase letters. The figures were generated with *PyMOL*.

Asp97(79) (which accepts the proton from the Schiff base) without unfavorable energetics involving His75(57), *i.e.* the replacement of an [N···H—O$^-$] hydrogen bond by an (:N···H—O) hydrogen bond. The W34(16)D mutation may stabilize the protonation of His75(57) ND1, thereby lowering the pK_a of Asp97(79) and inhibiting the Schiff-base proton transfer to this residue.

Sequence alignment and analysis showed that all PR sequences with Gln105(87) (*i.e.* BPRs) have a conserved Trp34(16), while the residues at position 34(16) vary in the PRs lacking a glutamine at position 105(87) (*e.g.* GPRs). This further suggests that this inter-protomer interaction [His75(57)–Trp34(16)] is conserved in BPRs.

The ion-pumping mechanism of PR needs to be investigated further, but several features are clear from the PR structures. Firstly, the proton-release region is different from BR and XR and is likely to involve only one glutamate instead of the two seen in BR. Secondly, the oligomeric states differ between PR and BR, featuring a novel intermolecular hydrogen bond between His75(57) of one protomer and Trp34(16) of a neighboring protomer. Thirdly, Wat402 is absent or is not well ordered in our BPR structures, suggesting a different mechanism by which a proton is transferred from the Schiff base to Asp97(79). The high-resolution crystal structures of two BPR variants now allow a structural comparison between the proton pumps in archaea and those found in bacteria.

Both *Med12*BPR and *HOT75*BPR variants of PR display oligomeric states that are different from that of BR. While BR typically forms a trimer, *Med12*BPR forms a hexamer, while *HOT75*BPR assembles into a pentamer. In BR, each protomer is able to transport ions on its own and there is no clear evidence that oligomerization is necessary for this activity. Our crystal structures revealed a possible role for oligomerization in PR because a hydrogen bond between Trp34(16) of one protomer and His75(57) of a neighboring promoter extends the counterion from the primary proton acceptor Asp97(79). Variants of PR have been noted for their high pK_a of Asp97(79) and it is possible that the inter-protomer hydrogen bond helps to lower the pK_a of Asp97(79) so that it is deprotonated at the beginning of the photocycle. Additionally, the proton-release region is different from BR. An ordered Wat402, a key structural water in BR responsible for transporting the proton from the Schiff base to Asp85, is missing in all three PR crystal structures, although there is very weak electron density in this region. The lack of this water remains a puzzle because Asp97(79) in PR is not sufficiently close to the Schiff base for direct proton transfer. A possibility is that Asp227(209) (Asp212 in BR) could play this role, but it is stabilized by two flanking tyrosine residues, similar to BR. Alternatively, the water may be present but too disordered to yield clear electron density. Further investigation is necessary, and structures of intermediate steps of PR would be beneficial in further explaining the similarities and differences between the BR and PR photocycles. Additionally, disruption of the oligomeric state of PR through site-directed mutagenesis would allow studies and photocurrent measurements of individual protomers for comparison with the oligomer.

GY and RT cloned, expressed, purified, crystallized and collected data for both *Med12*BPR and *HOT75*BPR. Initial crystallization results for *HOT75*BPR have been published in Wang *et al.* (2012). RT used SeMet *HOT75*BPR crystals to perform phasing. GO and HL performed data processing, model building and structure refinement for *Med12*BPR. GO performed additional model building and refinement of *HOT75*BPR. OAS conducted the *in vivo* photocurrent measurements. WW, HL and JLS directed the project during different phases and HL, GO, WW and JLS wrote the manuscript. We are grateful to the staff members of the Swiss Light Source and the Shanghai Synchrotron Radiation Facility for help with data collection. R37GM027750 (JLS), endowed chair AU-0009 from the Robert A. Welch Foundation (JLS) and grants from the National Natural Science Foundation of China (30700135 and 31170686), 'The Fundamental Research Funds for the Central Universities' (WW), are acknowledged. Ikerbasque is thanked for a part-time Research Professorship.

References

Adams, P. D. *et al.* (2010). *Acta Cryst.* D**66**, 213–221.
Balashov, S. P., Petrovskaya, L. E., Lukashev, E. P., Imasheva, E. S., Dioumaev, A. K., Wang, J. M., Sychev, S. V., Dolgikh, D. A., Rubin, A. B., Kirpichnikov, M. P. & Lanyi, J. K. (2012). *Biochemistry*, **51**, 5748–5762.
Béjà, O., Aravind, L., Koonin, E. V., Suzuki, M. T., Hadd, A., Nguyen, L. P., Jovanovich, S. B., Gates, C. M., Feldman, R. A., Spudich, J. L., Spudich, E. N. & DeLong, E. F. (2000). *Science*, **289**, 1902–1906.
Béjà, O., Spudich, E. N., Spudich, J. L., Leclerc, M. & DeLong, E. F. (2001). *Nature (London)*, **411**, 786–789.
Bergo, V. B., Sineshchekov, O. A., Kralj, J. M., Partha, R., Spudich, E. N., Rothschild, K. J. & Spudich, J. L. (2009). *J. Biol. Chem.* **284**, 2836–2843.
Cartailler, J.-P. & Luecke, H. (2004). *Structure*, **12**, 133–144.
Dioumaev, A. K., Brown, L. S., Shih, J., Spudich, E. N., Spudich, J. L. & Lanyi, J. K. (2002). *Biochemistry*, **41**, 5348–5358.
Dioumaev, A. K., Wang, J. M., Bálint, Z., Váró, G. & Lanyi, J. K. (2003). *Biochemistry*, **42**, 6582–6587.
Emerson, S. & Hedges, J. (2008). *Chemical Oceanography and the Marine Carbon Cycle.* Cambridge University Press.
Emsley, P., Lohkamp, B., Scott, W. G. & Cowtan, K. (2010). *Acta Cryst.* D**66**, 486–501.
Faham, S. & Bowie, J. U. (2002). *J. Mol. Biol.* **316**, 1–6.
Friedrich, T., Geibel, S., Kalmbach, R., Chizhov, I., Ataka, K., Heberle, J., Engelhard, M. & Bamberg, E. (2002). *J. Mol. Biol.* **321**, 821–838.
Hempelmann, F., Hölper, S., Verhoefen, M.-K., Woerner, A. C., Köhler, T., Fiedler, S.-A., Pfleger, N., Wachtveitl, J. & Glaubitz, C. (2011). *J. Am. Chem. Soc.* **133**, 4645–4654.
Humphrey, W., Dalke, A. & Schulten, K. (1996). *J. Mol. Graph.* **14**, 33–38.
Kabsch, W. (2010). *Acta Cryst.* D**66**, 125–132.
Klyszejko, A. L., Shastri, S., Mari, S. A., Grubmüller, H., Muller, D. J. & Glaubitz, C. (2008). *J. Mol. Biol.* **376**, 35–41.
Krissinel, E. & Henrick, K. (2004). *Acta Cryst.* D**60**, 2256–2268.
Laskowski, R. A., Moss, D. S. & Thornton, J. M. (1993). *J. Mol. Biol.* **231**, 1049–1067.
Luecke, H., Schobert, B., Lanyi, J. K., Spudich, E. N. & Spudich, J. L. (2001). *Science*, **293**, 1499–1503.
Luecke, H., Schobert, B., Richter, H.-T., Cartailler, J.-P. & Lanyi, J. K. (1999). *J. Mol. Biol.* **291**, 899–911.

Luecke, H., Schobert, B., Stagno, J., Imasheva, E. S., Wang, J. M., Balashov, S. P. & Lanyi, J. K. (2008). *Proc. Natl Acad. Sci.* **105**, 16561–16565.
Man, D., Wang, W., Sabehi, G., Aravind, L., Post, A. F., Massana, R., Spudich, E. N., Spudich, J. L. & Béjà, O. (2003). *EMBO J.* **22**, 1725–1731.
McCoy, A. J., Grosse-Kunstleve, R. W., Adams, P. D., Winn, M. D., Storoni, L. C. & Read, R. J. (2007). *J. Appl. Cryst.* **40**, 658–674.
Michel, H. (1983). *Trends Biochem. Sci.* **8**, 56–59.
Reckel, S., Gottstein, D., Stehle, J., Löhr, F., Verhoefen, M., Takeda, M., Silvers, R., Kainosho, M., Glaubitz, C., Wachtveitl, J., Bernhard, F., Schwalbe, H., Güntert, P. & Dötsch, V. (2011). *Angew. Chem. Int. Ed.* **50**, 11942–11946.
Rouhani, S., Cartailler, J.-P., Facciotti, M. T., Walian, P., Needleman, R., Lanyi, J. K., Glaeser, R. M. & Luecke, H. (2001). *J. Mol. Biol.* **313**, 615–628.
Sabehi, G., Loy, A., Jung, K.-H., Partha, R., Spudich, J. L., Isaacson, T., Hirschberg, J., Wagner, M. & Béjà, O. (2005). *PLoS Biol.* **3**, e273.
Schneider, T. R. & Sheldrick, G. M. (2002). *Acta Cryst.* D**58**, 1772–1779.
Shastri, S., Vonck, J., Pfleger, N., Haase, W., Kuehlbrandt, W. & Glaubitz, C. (2007). *Biochim. Biophys. Acta*, **1768**, 3012–3019.
Sheldrick, G. M. (2008). *Acta Cryst.* A**64**, 112–122.
Sheldrick, G. M. (2010). *Acta Cryst.* D**66**, 479–485.
Shi, L., Ahmed, M. A., Zhang, W., Whited, G., Brown, L. S. & Ladizhansky, V. (2009). *J. Mol. Biol.* **386**, 1078–1093.
Shi, L., Lake, E. M., Ahmed, M. A., Brown, L. S. & Ladizhansky, V. (2009). *Biochim. Biophys. Acta*, **1788**, 2563–2574.
Sineshchekov, O. A. & Spudich, J. L. (2004). *Photochem. Photobiol. Sci.* **3**, 548–554.
Spassov, V. Z., Luecke, H., Gerwert, K. & Bashford, D. (2001). *J. Mol. Biol.* **312**, 203–219.
Spudich, J. L., Yang, C.-S., Jung, K.-H. & Spudich, E. N. (2000). *Annu. Rev. Cell Dev. Biol.* **16**, 365–392.
Stone, K. M., Voska, J., Kinnebrew, M., Pavlova, A., Junk, M. J. N. & Han, S. (2013). *Biophys. J.* **104**, 472–481.
Strugatsky, D., McNulty, R., Munson, K., Chen, C.-K., Soltis, S. M., Sachs, G. & Luecke, H. (2013). *Nature (London)*, **493**, 255–258.
Wang, N., Wang, M., Gao, Y., Ran, T., Lan, Y., Wang, J., Xu, L. & Wang, W. (2012). *Acta Cryst.* F**68**, 281–283.
Wang, W.-W., Sineshchekov, O. A., Spudich, E. N. & Spudich, J. L. (2003). *J. Biol. Chem.* **278**, 33985–33991.
Winn, M. D. *et al.* (2011). *Acta Cryst.* D**67**, 235–242.